International Journal of Engineering Research and Technology. ISSN 0974-3154, Volume 12, Number 7 (2019), pp. 1064-1074

Design and Wall Fluid Parameters Evaluation of the Dual-Bell Nozzle

T. Hamitouche [1,*], M. Sellam [2], H. Kbab[3] and S. Bergheul[4]

[1, 3, 4] Laboratoire des Sciences Aéronautique, Institut d`Aéronautique et des Etudes Spatiales, Université de Blida1, BP 270, Route de Soumâa, Blida.

[2] Laboratoire de Mécanique et d'Energétique d'Evry ; 40 rue du Pelvoux 91020 EVRY Courcouronnes Cedex.

** Corresponding authors*

[1]ORCID: 0000-0003-1960-662X, [2]ORCID: 0000-0002-0021-0951

Abstract

The dual-bell nozzle is an innovating-technology of Rocket Nozzles; it is one of the most promising concepts for the altitude-compensating nozzles. Indeed, the flow in this type of nozzle has the ability to auto-adapting for both operating modes (Sea-Level Mode and High-Altitude Mode) without mechanical activation. The principle is theoretically simple but structural forces involved can be significant. In this study, the numerical method proposed for the design of the dual bell profile is based on: the inverse method of characteristics for the first bell and the direct method of characteristics applied for a free jet for the second bell. We were also interested in the thermodynamic-parameters evolution (pressure, Mach number, temperature, density…) and aerodynamic performances (thrust, specific impulse...) along the nozzle in order to validate our step thereafter.

For more consistency, a numerical simulation of flows in the obtained dual bell nozzles is achieved using a computer code ANSYS. The computed results are compared to the experimental works of: the National Office of Studies and Aerospace Research (ONERA-France) and the National Space Research Center (CNRS-Orleans). The comparison of the different studied configurations (Ideal, TIC and Dual-Bell) is limited to the performances and the diverging dimensions (length and radius). The obtained results show a good concordance.

Keywords: CFD; Dual bell nozzles; Innovating nozzles; Method of characteristics; Nozzles design; Supersonic flows; Transition.

1. INTRODUCTION

Within the framework of research on the effective nozzles devoted to spatial propulsion, several concepts of nozzles (known as the Advanced Rocket Nozzles) have been developed. Among the latter, we find: the two-positions or the extendible nozzles, the plug nozzles (aerospike) and the dual bell nozzles. This last concept is based on the principle of forcing the flow to separate from the nozzle wall at a desired location by imposing an inflection point. This ensures a controlled and symmetrical separation (first operating mode (**Sea-Level Mode**) corresponding to the upper part shown in figure 1) allowing to minimize the side loads production.

During the climb in altitude, the ambient pressure decreases till it reaches a second pressure of adaptation enabling the flow to attach to the wall of the second profile (second operating mode (**High-Altitude Mode**) illustrated on the bottom part of the figure 1).

The efficiency of this new concept is to make available to researchers and manufacturers two operating modes: one at low altitudes (**Sea-Level Mode**) and another for high altitudes (**High-Altitude Mode**), without the contribution of any supplementary device to switch from a mode to another. As direct consequence: a reduction in the nozzle weight. This ability of auto-adaptation places it as one of the most promising concepts for the adaptable nozzles in altitude.

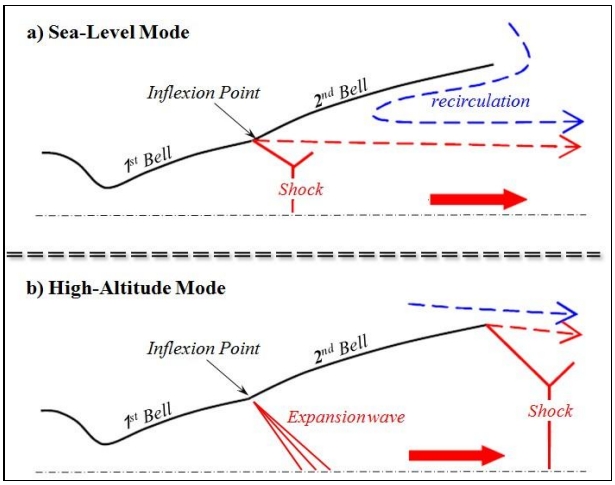

Fig. 1: Main operating modes of a dual bell nozzle.

The idea of dual bell nozzles has first been suggested in 1949 by FOSTER and COWLES **[1]**, but it is only from the Nineties that studies on this type of nozzles have been developed, we'll mention: for instance, the experimental works of HORN and FISHER achieved at Rocketdyne Division in (1994), the numerical studies of GOEL and JENSEN in (1995), IMMICH and CAPORICCI in (1996), HAGEMANN and ALL in (1997) **[2]**. So far, the study of this type of nozzles is a subject of actuality. Among the recent studies, that of the Kakuda Space Centre (of the Japanese agency JAXA) in (2003) which considers the use of this concept as a possible solution to increase the performances of

the space vehicle engines **[3]**. The parametric analysis of dual bell nozzle flows elaborated by MARTELLI, NASUTI and ONOFRI in (2007) **[4]** aimed to explore in detail the geometrical and physical parameters that affect the flow in the inflection region and that lead to the generation of side loads in this type of nozzles. This study allowed the authors to study later (in 2009) the transition in these nozzles **[5]**. In 2011, they obtained promising results on the reduction of the transition time by using a secondary gas injection **[6]**. At the DLR of Germany, C.Génin and R.Stark **[2, 7-11]** have also largely studied and obtained promising results on the transition between the two operating modes of the dual bell nozzles and the side loads which accompany it.

Within the CNES-PERSEUS program, Reijasse and all **[12]** tested on wind tunnel a dual bell nozzle which can be used in the future for the nanosatellite launchers. The tests were achieved at the ONERA-R2Ch wind tunnel in 2009. In 2013, Verma conduce an experimental investigation to study the Reynolds number influence on dual-bell transition behavior for tests inside a high-altitude simulation chamber**[13]**. He particularly studied its influence on the flow behavior in the region of wall inflection and its accompanied affect on the transition duration.

Recently, in 2014, K.Davis and all **[14]** of Worcester Polytechnic Institute (U.S.A), have proposed a conception process of the dual bell nozzle profile for an application on a cube-satellite (CubeSat) launch vehicle called Nanolaunch 1200. Their study aims to reduce the cost of placing a 3-U CubeSat into low Earth orbit. At the conclusion of their tests and simulations, they recommend changing the location of the contour inflection point while optimizing the design point pressure ratios.

In order to evaluate the impact of dual bell nozzles for the Ariane 5 ECA on the payload mass delivered into geostationary transfer orbit (GTO), D.Schneider and all **[15]** have used two different techniques, an analytical approach based on the rocket equation and a detailed launch vehicle trajectory simulation. They found an payload mass increase around 450 kg; this means a increase of around 4.5 %, assuming a cost of approximately 16000 Euro per kg payload into GTO. In 2016, with C.Génin, D.Schneider investigates the influence of different turbulence models and feeding pressure gradients on the flow transition behavior of a dual-bell nozzle with positive pressure gradient extension**[16]**.

In Algeria, at the Aeronautical Sciences Laboratory (LSA-IAES), in collaboration with the Mechanics and Energetic Laboratory of the University of Evry (LMEE), an investigation on the designing method and performance evaluation of the dual bell nozzles was conduced **[17-19]**. Kbab and al. **[18]** performed the numerical method to develop the dual bell nozzle. The direct method of characteristics has been used to draw the base nozzle profile and the extension wall.

For our study, the purpose is to present the profiles of the supersonic nozzles particularly the dual bell nozzles by the method of characteristics (MOC), also to determine the behavior of the fluid parameters (pressure, Mach number, temperature and density) along the wall of these nozzles. To this end, a computer code was developed within the laboratory of aeronautical sciences (LSA-IAES) **[19]**. The second part of the study is reserved to the numerical simulation of the flows in this type of nozzles using the CFD. Different types of mesh are generated by Ansys-ICEM 15.0. The non viscous and viscous calculations are carried out under Ansys-Fluent 15.0 environment. The obtained results are compared to those of the other references (ONERA **[12]** and CNRS **[20]**).

2. CONCEPTION METHOD (DESIGN) OF A DUAL BELL NOZZLE CONTOUR

During our present work, the calculations are made with a perfect gas. The profile chosen for the implementation of the method of characteristics is the one describing the divergent section of an axisymmetric bell nozzle.

The design of the dual bell nozzle is carried out in two parts:

2.1 First contour (base nozzle) design

The base nozzle profile is the one of a Truncated Ideal Contour (TIC nozzle) obtained by truncating an Ideal nozzle calculated to generate a parallel flow (axial flow) at its exit. The profile of the latter is obtained by applying the inverse method of characteristics (figure 2) for: a design Mach number (M_d) equal to 3.2, a throat radius y_t = 0.01 m and a total exit radius of 0.0226 m **[19]**.

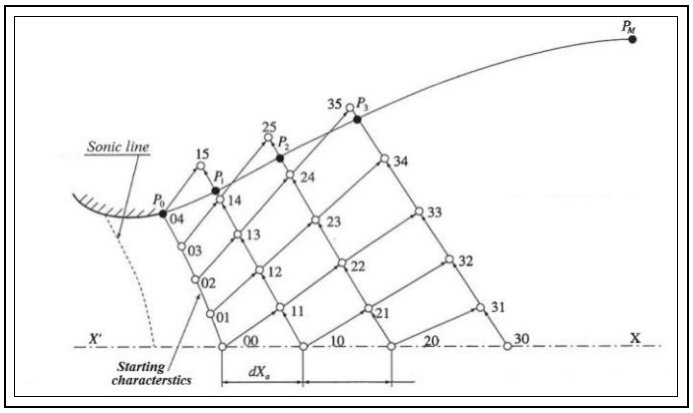

Fig 2: The inverse method of characteristics calculation process [21].

The flow $\dot{m}_0$ crossing the starting characteristic ξ_0 (at the throat) is given (for a symmetrical flow) by the following equation:

$$\dot{m}_0 = 2\pi \int_0^{P_0} \rho.a.y.d\xi \qquad (1)$$

Where: $\boldsymbol{\rho}$: the density

$\boldsymbol{a}$: the speed of sound

$\boldsymbol{y}$: the ordinate of the point P on $\boldsymbol{\xi_0}$

The wall being a streamline, its position is obtained by respecting the criteria of the mass flow rate conservation (**eq 2**) between the sections to the throat and in the P_n point on the calculated ξ characteristic **[21]**:

$$2\pi \int_0^{Pn} \rho.a.y.d\xi = \dot{m}_0 \qquad (2)$$

Considering that our computer calculation code is based on the method of characteristics (MOC), a slightly supersonic initial line is indispensable; this one is generated by the Sauer's approach **[22]**, see figure 3 below.

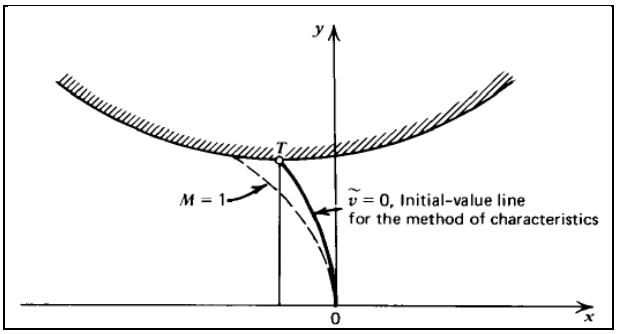

Fig 3: Initial line for the method of characteristics [23].

The method of Sauer is based on the theory of the small perturbation. Perturbation equation at the throat (for a 1D sonic flow) is then written:

$$(\gamma+1)u'u'_x - v'_x - \delta\frac{v'}{y} = 0 \qquad (3)$$

Where:

$u' = \frac{u}{a^*}$ **and** $u' = \frac{u}{a^*}$ are the perturbation speed components;

a^* : the speed of sound at the throat;

δ : Switch (δ = 0 for a plane flow

and δ =1 for an axisymmetric flow)

Otherwise, the critical curve where M=1 is defined by the following expression:

$$x = -\frac{(\gamma+1).\alpha.y^2}{2(1+\delta)} \qquad (4)$$

As for the origin of the coordinate system relating to the nozzle throat, it is localized by the following expression:

$$\varepsilon = -\frac{(\gamma+1).\alpha.y_t^{\,2}}{2(1+\delta)} \qquad (5)$$

The running of our calculation code requires a set of additional data, in complement to the aforementioned data. The table 1 groups the thermodynamic and geometrical data used during our calculations to draw the profile of the base nozzle.

Table 1: Thermodynamic and geometrical data of the base nozzle profile.

Quantities	**Values**
Throat radius y_t , **m**	0.01
Chamber temperature T_t , **K**	243
Chamber pressure P_t , **bars**	30
Ideal nozzle exit radius y_{Id}, **m**	0.0226
Truncation length $L_{TIC} = L_1$, **m**	0.0868
Design Mach number M_d	3.2
Ambient pressure p_1 , **bars**	1.013
Specific heat ratio γ	1.4

The advantage of the method of characteristics is that as the calculation of the profile proceeds, the mesh of the inner domain of this last one is generated. Figure 4 presents the profile (in red) of the Ideal nozzle carried out by our computer code with its mesh (in green). The comparison between our profiles (Ideal and TIC) and those of the CNRS **[20]** obtained for the same data is illustrated on the figure 5.

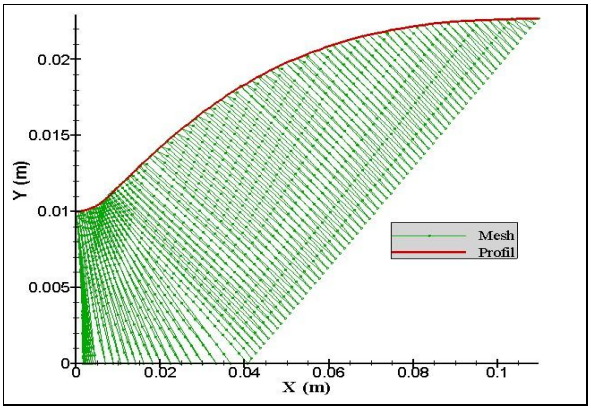

Fig. 4: The obtained Ideal nozzle contour for M_d = 3.2 and its mesh.

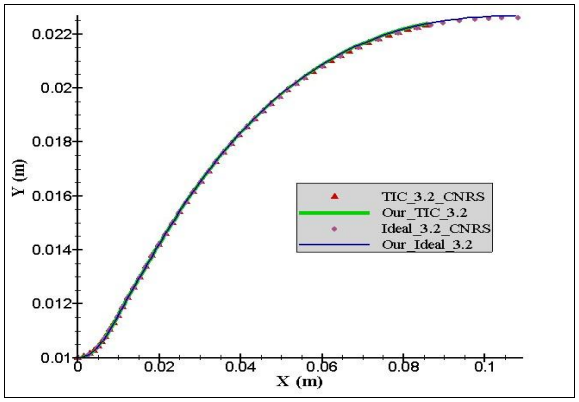

Fig. 5: Comparison between our obtained profiles and those of the CNRS.

From figure 4, the mesh occupies the entire internal flow field in the expansion zone (kernel zone). From the exit of this last, a Mach line named of design is extended, this line joins the two points: that of the kernel area's end (at 0.04 m from the throat on the axis of symmetry) and the point which is located at the edge of the nozzle that is at 0.109 m of abscissa from the throat. The part not meshed (down the line of design) constitutes an area in which the flow is completely parallel to the axis of symmetry and all its parameters remain constant and equal to the parameters at the edge of the Ideal nozzle. Therefore, during our present study, we will be only interested to the parietal parameters.

A very good agreement is observed on the profiles of the configurations (Ideal and TIC; see figure 5).

Figures 6 and 7 present the comparison of the wall parameters (pressure ratio, Mach number, temperature and density) of our computed Ideal nozzle to those of the CNRS Ideal nozzle.

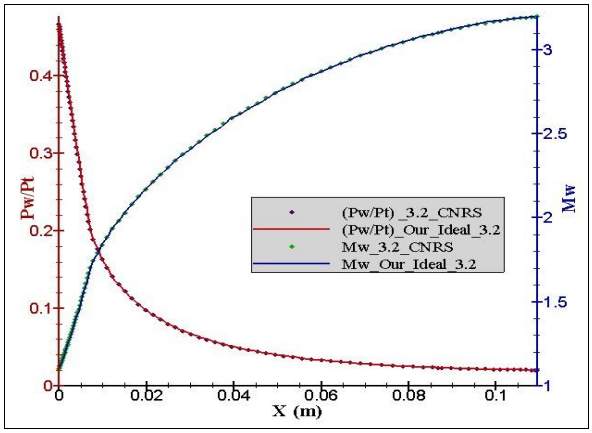

Fig. 6: Evolution of the wall pressure ratio and wall Mach number.

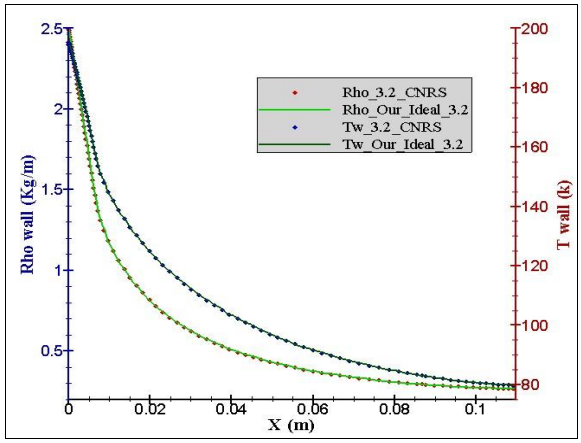

Fig. 7: Evolution of the temperature and the density on the ideal nozzle wall.

According to figure 6, the wall Mach number evolves very quickly on the expansion area to reach the value of 1.70. Beyond, we notice a slower progression in the divergent part until reaching the value of the design Mach 3.2 at the edge of nozzle. This evolution is accompanied by a fast decrease of the wall pressure ratio, the wall density (see figure 7) and temperature which reach respectively: $0.02*P_t$, 0.29 Kg/m and 82.78 K at the edge of the nozzle.

We also notice a perfect agreement between the obtained results and those experimental of CNRS.

It should be noted that the truncation of this Ideal nozzle is made at the X-coordinate x= 0.868 m in order to respect the CNRS conditions on the Mach number value that should be reached at the TIC nozzle exit which is equal to 3.104.

2.2 Second bell (nozzle extension) design

The second bell (nozzle extension) contour is calculated to give a constant wall pressure $\boldsymbol{P_2}$ (free jet). This is achieved by using the direct method of characteristics applied for a centered expansion wave (Prandtl-Meyer wave) that the intensity is $\boldsymbol{P_2/P_1}$ at the junction point ***J*** (see figure 8 below).

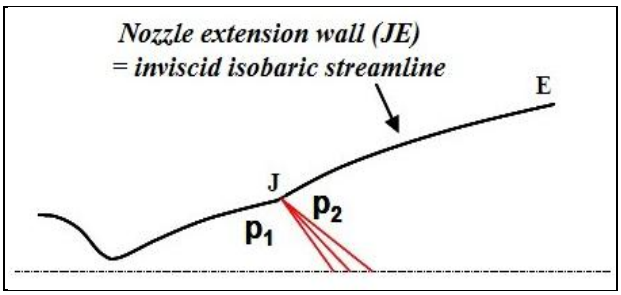

Fig. 8: Centered expansion at the junction point J [12].

Knowing that the second contour is only the expansion of the first contour, data used for its calculation, in addition to those of table 1 are: the inflection angle $AA_2 = 7.2°$ used by the DLR German center to represent their two profiles DB1 and DB3 **[9]**, the second adaptation pressure $\boldsymbol{p_2} = 0.02488$ **bars**, as well as the second contour length $L_2 = 0.0304$ m.

The dual bell nozzle (DBN) profile generated by our calculation code as the evolution of the different parameters (pressure ratio, Mach number, temperature and density) along its wall are illustrated on figures 9 and 10 respectively.

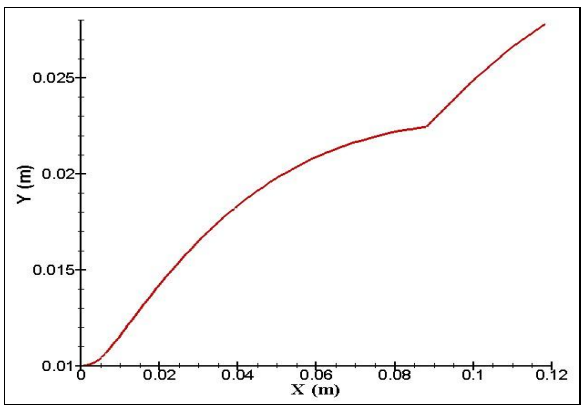

Fig. 9: Dual bell nozzle profile.

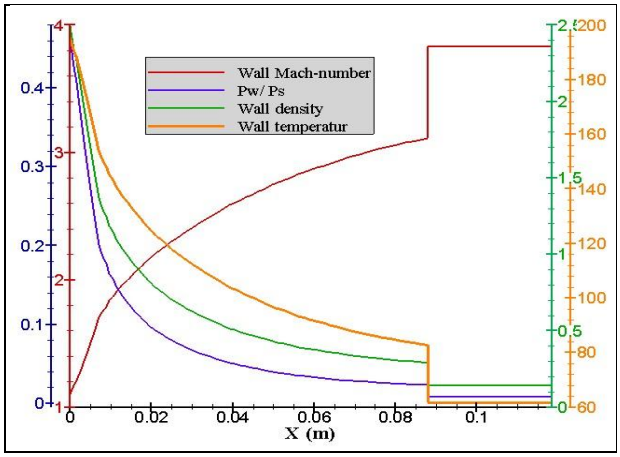

Fig. 10: Evolution of the wall parameters of the DBN.

On figure 9, there is a discontinuity on the contour slope at x = 0.086 m to the throat; it's the inflection point where the two profiles (the ones of the 1st bell and the ones of the 2nd bell) are joined. We note this point (also called the junction point) by the letter "***J*** " during the analysis of our results.

2.3 Discussion of the flow parameters evolution along the DBN wall

As it can be seen in figure 10, the evolution of the different wall parameters (pressure ratio, density, temperature and Mach number) in the first bell (base nozzle) is the same as the Ideal nozzle. Their values reached at the exit of the first bell (junction point) are respectively: 0.02*P_t, 0.29 Kg/m, 82.78 k, and 3.1.

At the junction point ***J***, the centered expansion wave is apparent. It leads to a sudden wall pressure drop reaching the imposed pressure value: 0.02488 bars (0.00829*P_t). This sudden drop in the wall pressure is accompanied by a drop in the wall temperature, the wall density and a jump in the wall Mach number which reaches respectively: 61.8 K, 0.14 Kg/m and 3.83. Beyond the junction point, all wall parameters remain constant along the second curve and preserve the same values aforementioned.

The table 2 presents the performances of the dual bell nozzle (DBN) obtained by using our calculation code.

Tableau 2 : Calculated dual bell nozzle performances.

Quantities	**Values**
Developed thrust F, **N**	147.29
Masse flow rate $\dot{m}$, **Kg/s**	0.24437
Nozzle discharge coefficient C_d	0.99723
Thrust coefficient C_f	1.56
Exit Mach number M_e	3.83
Specific impulse I_s , **N.s/Kg**	602.726

3. VALIDATION TEST

In order to validate our computer code, we have carried out the calculation of the profile of a real dual bell nozzle belonging to the CNES-PERSUS program **[12]**. Table 3 regroups all the data extracted from the reference **[12]** to draw the profile of this dual bell nozzle.

Table 3: Thermodynamic and geometrical data of the DBN profile according to ref [12].

Quantities	**Values**
Throat radius y_t, **m**	0.01
Chamber temperature T_t, **K**	330
Chamber pressure P_t, **bars**	52
Ideal nozzle exit radius y_{Id}, **m**	0.03106
Truncation length $L_{TIC} = L_1$, **m**	0.08833
2nd bell length L_2, **m**	0.1767
1st bell design Mach number M_d	3.9
1st bell ambient pressure p_1, **bars**	0.651
2nd bell ambient pressure p_2, **bars**	0.065
Specific heat ratio **γ**	1.4

The new calculated DBN profile as the evolution of the different wall parameters (pressure ratio, Mach number, temperature and density) are presented respectively on figures 11 and 12.

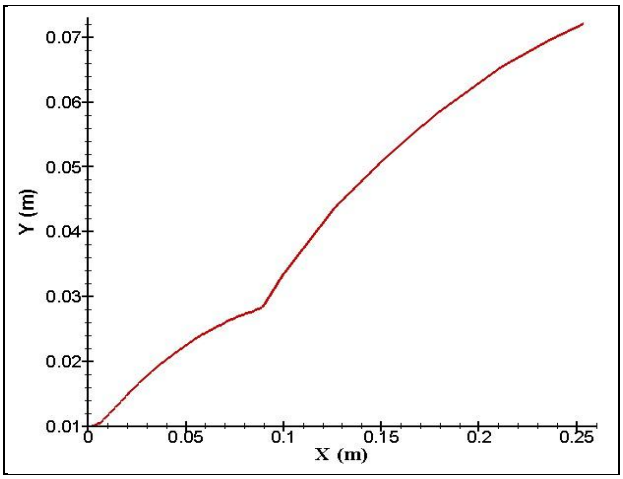

Fig. 11: Calculated DBN profile according to ref [12] data.

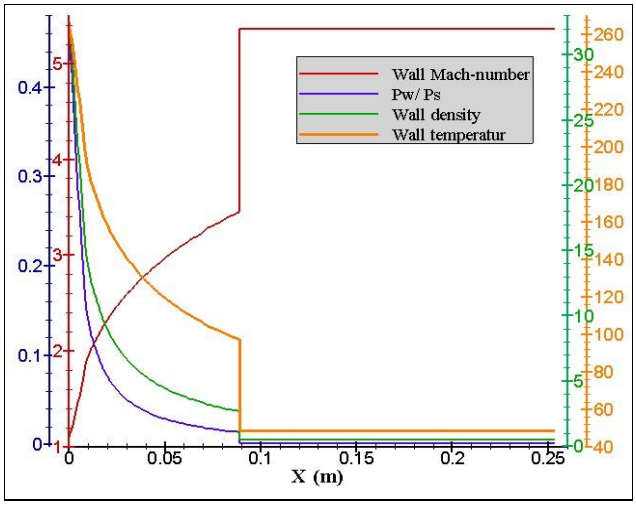

Fig. 12: Evolution of the parietal parameters of the obtained DBN.

3.1 Discussion of the flow parameters evolution along the DBN wall:

The Mach number increases rapidly at the expansion zone to reach the value of 1.85. But, in the divergent part forming the 1st bell, this evolution is less fast; it reaches the value of 3.45 at the exit of this curve. This evolution is accompanied by a fast decrease of the wall pressure ratio (see Fig. 12), the wall density and temperature. Their values at the edge of the base nozzle (point ***J***) are: 0.014*P_t, 2.67 Kg/m and 97.53 **K** respectively.

At the junction point ***J***, the pressure drops suddenly (thus forming an expansion fan) until reaching the imposed pressure value 0.065 bars (0.00125*P_t). This drop in the wall pressure is accompanied by a drop in the wall temperature, and wall density and a raise in the wall Mach number which reaches: 48.87 **K**, 0.48 Kg/m and 5.36 respectively. Beyond the junction point, all wall parameters remain constant along the second curve and preserve the same values mentioned previously.

3.2 Comparison to the reference [10] results

Table 4 shows the comparison between the MOC results and those presented in the reference **[12]**.

The error shown in the last column of Table 4 is a relative error calculated using the following formula:

$$E = \frac{\text{Reference [12] results - Our results}}{\text{Reference [12] results}} \times 100 \qquad (6)$$

Table 4: Comparison of our results to those of reference [12].

Quantities	Our results	Ref. [12] Results	Error (%)
Isentropic pressure ratio at the exit of the 1st bell P_1/P_t	0.0140	0.01252	11.82
Isentropic pressure ratio at the exit of the DBN P_2/P_t	0.00125	0.00124	0.80
Exit Mach number of the 1st bell M_{e1}	3.452	3.533	2.29
Exit Mach number of the DBN M_{e2}	5.36	5.34	0.37
Normalized specific impulse of the 1st bell Isp_1/Isp_{th}	1.218	1.282	4.99
Normalized specific impulse of the DBN Isp_2/Isp_{th}	1.326	1.306	1.53
1st bell length L_1/R_{th}	8.903	8.833	0.79
Dual bell nozzle length L_2/R_{th}	25.34	26.51	4.41
1st bell exit radius y_1/R_{th}	2.827	2.879	1.81
Dual bell nozzle exit radius y_2/R_{th}	7.21	7.46	3.35

By analyzing the table 4 values, we can see a good coherence between our results and those of the reference **[12]** seen that the relative error is less than 3 %. This is valid for all results except for the isentropic pressure ratio at the exit of the 1st bell P_1/P_t where the relative error is estimated at 11.82 %.

The performances of this second nozzle are evaluated by our computer code and are summarized in Table 5:

Table 5: Evaluated new DBN performances.

Quantities	Values
Developed thrust F, N	2720.85
Masse flow rate $\dot{m}$, Kg/s	3.6799
Nozzle discharge coefficient C_d	0.99723
Thrust coefficient C_f	1.67
Exit Mach number M_e	5.36
Specific impulse I_s, $N.s/Kg$	739.379

4. NUMERICAL SIMULATIONS OF FLOWS IN THE DUAL BELL NOZZLE

The second validation test is devoted to the numerical simulation of flows inside the generated dual bell profile. The simulation results are compared to those provided by the method of characteristics.

The generation of the mesh is of main importance as for the success of calculations and to the results precision. It strongly differs according to the problem and calculations that we wish to run. It serves for the discrete representation of the continuous variables. However, a good mesh results from a compromise between the required precision and the computing time.

Several sizes of mesh are used to study the independence of the obtained results. These meshes are refined in the areas of the throat and near the wall (areas where the local properties of the flow vary quickly).

4.1 Inviscid calculation:

The mesh used for calculations of the 2D non-viscous flow is a structured multi-blocks mesh. A number of 450 nodes have been distributed on the nozzle divergent wall. The mesh includes 44352 quadrilateral cells.

Figure 13 illustrates the contour of Mach in the dual bell nozzle by applying the boundary conditions previously defined (i.e. non-viscous Euler calculation) on our model implemented in Fluent.

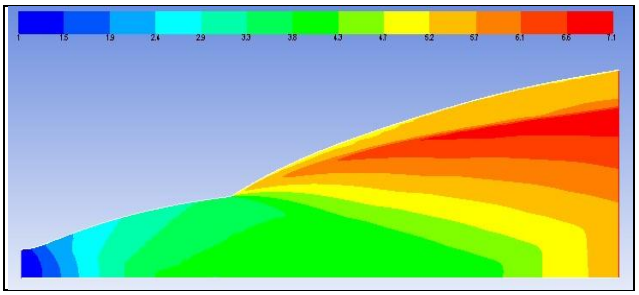

Fig. 13: The obtained Iso-Mach Contour for DBN.

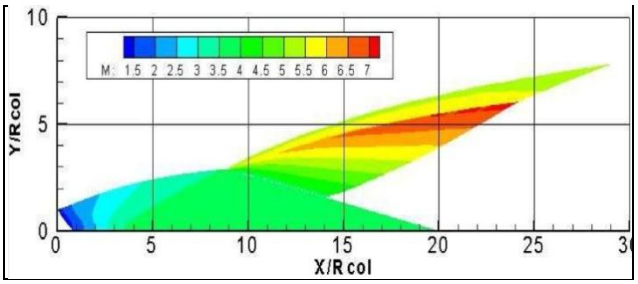

Fig. 14: Contour of Mach in the DBN provided by [12].

On the figure 13, the flow is perfectly attached to the nozzle walls which indicates the absence of separation. According to the pressure contours (which are not presented here), it is the non formation of an internal shock. It should be noted, that this nozzle has been optimized for a pressure ratio (NPR) equal to 800.

Figure 14 above presents the contour of Mach in the dual bell (DBN) profile provided by the reference [12]. The comparison of both contours gives a total satisfaction, because the form of both contour of Mach is perfectly coherent.

4.2 Viscous calculations and the transition study:

The CFD calculations offer the possibility to simulate real cases and often with a high precision. Physically, the nozzle-jet always emerges in an infinite atmosphere whose *conditions of pressure and temperature* condition *its operating mode*.

During the present viscous calculations, the ambient conditions around the nozzle were modeled by applying a computational domain of $33R_{th}$ in the x-direction by $21R_{th}$ in the y-direction. For the modeling of the flow turbulence, two models have been adopted, namely: Kw-SST and Spalart-Allmaras.

To show the grid independence of the obtained results, two multi-blocs structured meshes refined near the wall were chosen:

- **Mesh A** of 29 118 quadrilateral cells;
- **Mesh B** constituted of 118 048 quadrilateral cells.

Figure 15 depicts the wall pressure variation obtained by the mesh A and B with as imposed conditions: NPR = 80 and the Kw-SST turbulence model. The analysis of these two results shows: the best solution is obtained with the mesh B because of the fluctuations noticed along the curve obtained with mesh A.

Therefore, mesh B will be adopted for the rest of our simulations.

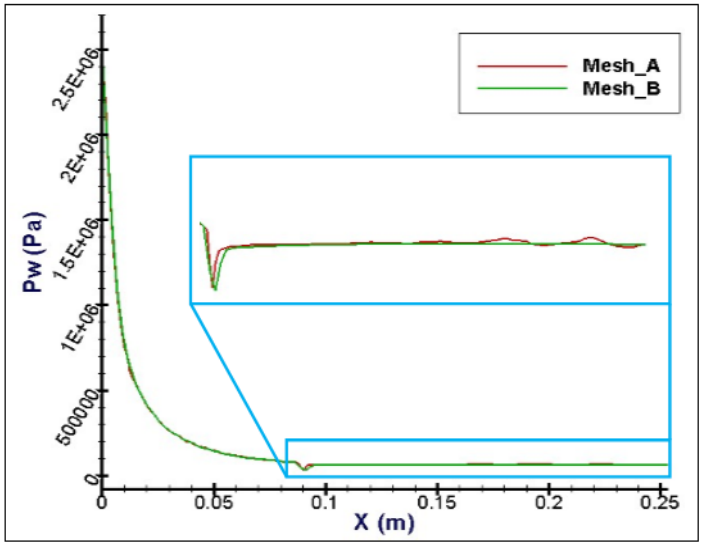

Fig.15: Comparison between mesh_A and mesh_B results for NPR=80.

A set of calculations was initiated to study the influence of the nozzle pressure ratios (NPR) variation over the dual bell nozzle operating mode, by focusing on the behavior of the fluid near the nozzle wall. The following conditions were taken into account during simulations:

- The NPR is linearly varied from 80 up to 280 in the case of the kw-SST turbulence model;

- For calculation using the Spalart-Allmaras model, the NPR is increased from 100 up to 200 with a step of 10.

In order to reproduce the physics of the studied problem accurately, the total feeding pressure was kept constant, while the ambient pressure was changed.

Figure 16 illustrates the mesh and the boundary conditions adopted.

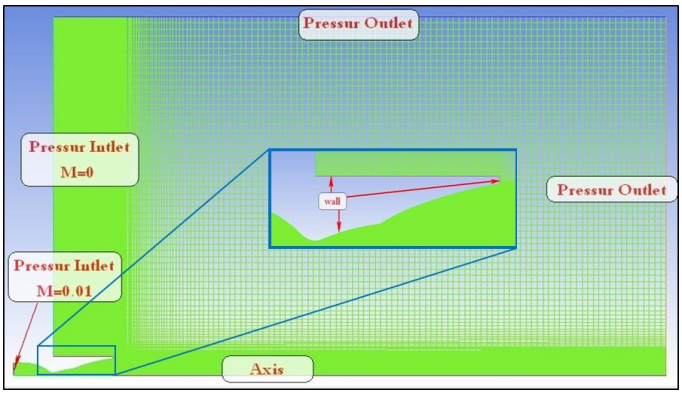

Fig. 16: Numerical computation domain, boundary conditions and adopted nozzle grid.

These simulations allowed us to highlight all operating modes of this nozzle while passing from **Sea-Level Mode** (figure 17.a), **Transition Mode** (figure 17.b) until the **High-Altitude Mode** (figure 17.c).

For each NPR result, the separation position of the dual bell nozzle flow was determined. Figure 18 illustrates the obtained positions of flow separation point according to NPR with the two models. The wall pressure variation according to NPR is shown in figures 19 and 20.

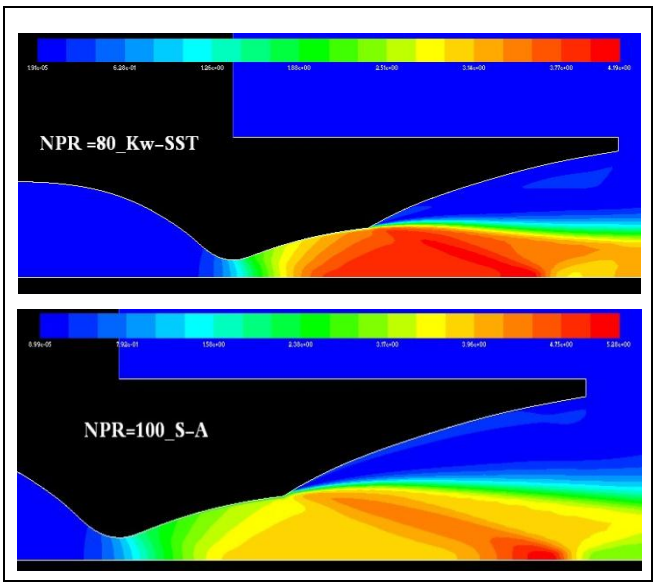

Fig. 17.a: Mach number distribution at Sea-Level Mode.

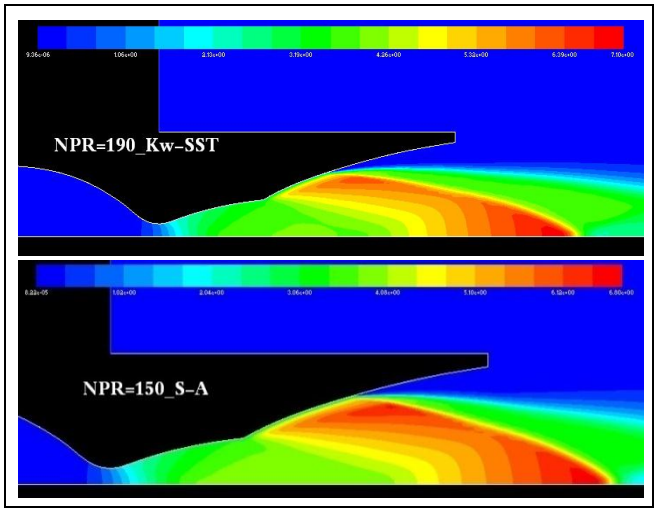

Fig. 17.b: Mach number distribution in Transition Mode.

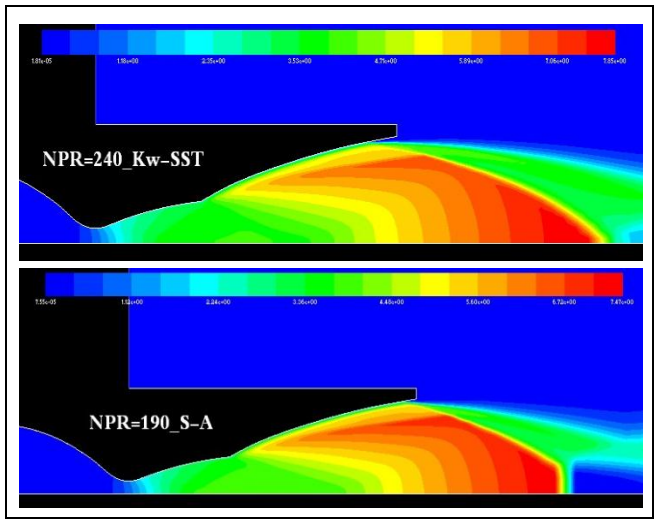

Fig. 17.c: Mach number distribution at High-Altitude Mode.

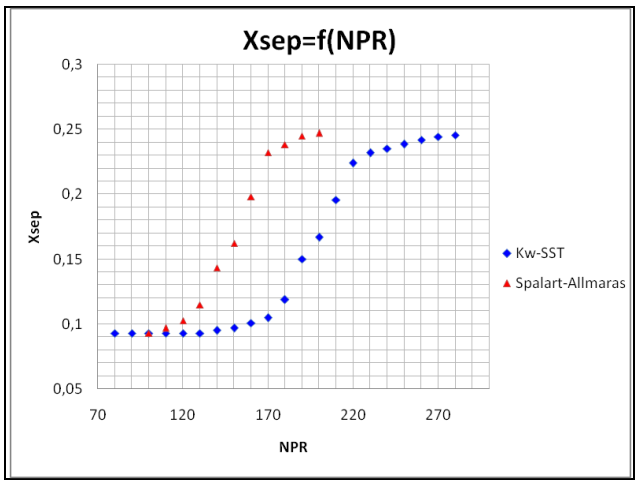

Fig. 18: Separation positions in a dual bell nozzle for different values of NPR.

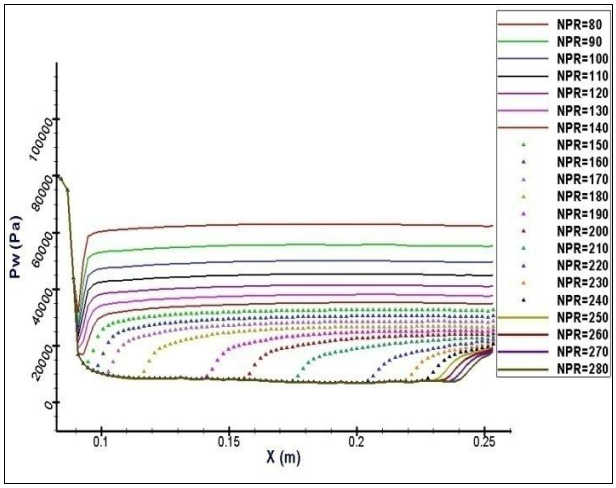

Fig. 19: Wall pressure distribution for different values of NPR applying the Kw-SST Model.

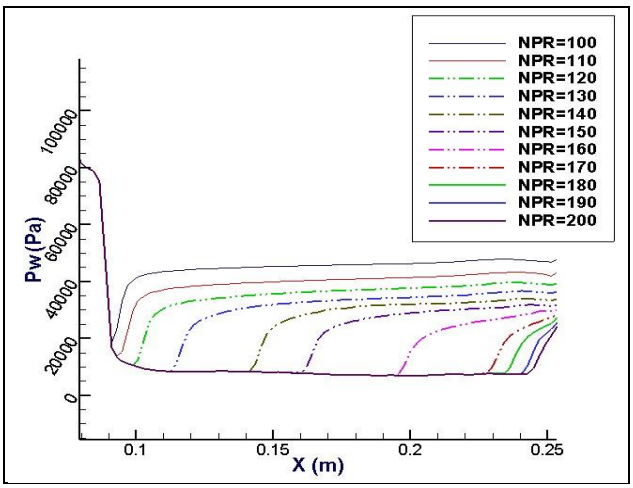

Fig. 20: Wall pressure distribution for different values of NPR applying the Spalart-Allmaras Model.

According to figure results, the nozzle operates in low altitude mode (Sea-Level Mode) for NPR ≤ 140; an abrupt raise of the wall pressure below the inflection point illustrates this. For NPRs contained between 150 and 240, we notice that the separation point crawls along the nozzle extension wall. Therefore, the nozzle operates during this phase in Transition mode.

The effective transition to high altitude mode is only reached from NPR = 240, the non-adaptation of the nozzle for this NPR value causes the flow detachment.

It should be noted that this profile is designed to be adapted at NPR=800. For NPR values greater than 240, the flow tends to attach to the nozzle's lip. On the other hand, according to the results obtained by using the Spalart-Allmaras model, the nozzle operates in sea level mode for NPR ≤ 110, and the effective transition to high altitude mode is reached at NPR = 180.

The results obtained by the ONERA's team **[12]** indicate that the same profile passes to the high altitude mode:

- At NPR= [138 – 144] for the experimental results;
- NPR=136 according to the Schilling criteria;
- NPR=153 according to the Schmucker criteria.

According to the Stark empiric criteria **[9]:**

$$NPR_{trans} = \frac{1}{M_e} \times \left(1 + \frac{(\gamma - 1)}{2} \times M_e^{\,2}\right)^{\frac{\gamma}{\gamma - 1}} = 149$$

The table below recapitulates our viscous simulation results and those obtained by the ONERA's team **[12]**.

Table 6: Comparison of our results to those of reference [12].

Our Results	Kw-SST	180 – 220
	Spalart-Allmaras	130 – 170
	Stark criteria	149
ONERA Results [12]	experimental results	138 – 144
	Schilling criteria	136
	Schmucker criteria	153

We notice a good concordance between our various results (especially those obtained by using the Spalart-Allmaras model) and the reference **[12]** results.

The wall pressure is an important parameter for the flows in the supersonic nozzles. Figure 21 presents its evolution along the DBN wall. The result obtained by the method of characteristics (MOC calculation) is compared to those of simulations (Euler calculation and viscous calculations).

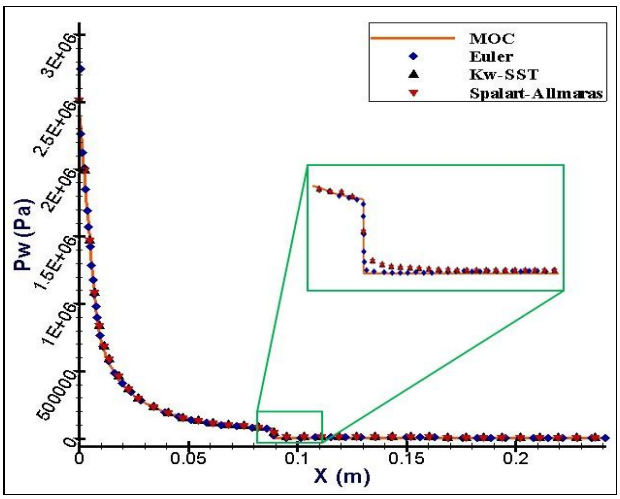

Fig. 21: Comparison between the wall pressure calculated by MOC and numerical simulations.

All curves show an isentropic expansion in the first bell. Approaching the point inflection (junction between the first and the second bell), a drop of pressure is noted. This fall is more marked in the case of MOC calculation. This can be explained by the centered Prandtl-Meyer expansion caused by the inflection of the nozzle profile. In the extension nozzle, all curves become constant until the exit of the nozzle. This result reveals the good design of the geometry of the dual bell profile.

5. CONCLUSIONS

The present study is devoted to the design of dual bell nozzles profile and the evaluation of their various wall parameters and performances by using the method of characteristics. For this purpose, a computer code in FORTRAN language was developed. To validate this last one, a numerical simulation of flow inside the obtained dual bell nozzle has been achieved. The non-viscous calculation allowed concluding the absence of shock wave formation in the obtained divergent. No detachment of flow is detected in this profile.

The computed results are represented in various curves: distributions of the pressure ratio, temperature, density and Mach number along the walls of the various studied configurations (namely: Ideal, TIC and dual bell). For all of the studied cases, the expansion of combustion gases occurs normally. It is made in a quick way along the throat downstream circular arc till the junction point (the end of the expansion zone). Beyond this last one, it progresses in less important way until reaching the exit of the first bell. At the junction, an expansion wave appears and leads the second curve to an adaptation pressure along this bell's wall.

In addition to inviscid simulation, we have compared the results of our calculation code to the experimental ones obtained by other studies (CNRS and ONERA). This comparison gives a very good agreement, owing to the fact that the results are very close.

The influence of the nozzle pressure ratios (NPR) variation over the dual bell nozzle operating mode has been studied using two turbulence models: Kw-SST and Spalart-Allmaras. The viscous calculation results were compared to those of ONERA, and a good agreement of the various results was observed.

These results suggest the advisability and desirability of such approach for the design of dual bell nozzles profile.

REFERENCES

[1] Foster and Cowles, "**Experimental Study of Gas Flow Separation in Overexpanded Exhaust Nozzles for Rocket Motors**". JPL Progress report 4-103, ***1949***.

[2] Génin, C. and Stark, R., "**Experimental Study of Dual Bell Nozzles** ", 2ND EUROPEAN CONFERENCE FOR AEROSPACE SCIENCES. ***2007***.

[3] JAXA/Kakuda Space Center web site, "**Combustor and Nozzle section** ", ***2003***.

[4] Martelli, E., Nasuti, F., and Onofri, M., "**Numerical Parametric Analysis of Dual-Bell Nozzle Flows**", AIAA Journal, Vol. 45, No. 3, ***2007***, pp. 640–650.

[5] Martelli, E., Nasuti, F., and Onofri, M., "**Film Cooling Effect on Dual-Bell Nozzle Flow Transition**", 45th AIAA/ASME/SAE/ASEE Joint Propulsion Conference & Exhibit, Denver, CO, AIAA 2009-4953, ***2009***.

[6] Martelli, E., Scaramuzzino, F., and Nasuti, F., "**Secondary Gas Injection Effect on Dual-Bell Nozzle Flow Transition**", 4TH EUROPEAN CONFERENCE FOR AEROSPACE SCIENCES. ***2011.***

[7] Génin, C. and Stark, R., "**Flow transition in dual bell nozzles**", Shock Waves, Vol. 19, pp. 265-270, Springer-Verlag, ***2009***.

[8] Stark, R. and Génin, C., "**Side loads in dual-bell nozzles, Part I Phenomenology**", 46th AIAA/ASME/SAE/ASEE Joint Propulsion Conference & Exhibit, ***25 - 28 July 2010***, Nashville, TN.

[9] Génin, C., "**Étude expérimentale de l'écoulement et des charges thermiques dans une tuyère dual-bell**", PhD thesis, Université de Valenciennes, France, ***2010***.

[10] Génin, C., Stark, R. and Schneider, D., "**Numerical investigation of Dual Bell Nozzle Flow Field**", 48th AIAA/ASME/SAE/ ASEE Joint Propulsion Conference & Exhibit, AIAA Paper 2012-4164, DOI: 10.2514/6. ***July 2012***.

[11] Génin, C., Stark, R. and Schneider, D., "**Transitional Behavior of Dual Bell Nozzles: Contour Optimization**", 49th AIAA/ASME/SAE/ASEE Joint Propulsion Conference & Exhibit, AIAA Paper 2013-3841, DOI: 10.2514/6. ***July 2013***.

[12] REIJASSE, P. and all, "**Wall Pressure and Thrust of a Dual Bell Nozzle in a Cold Gas Facility**", Progress in Propulsion Physics, Vol. 2, pp. 655-674, ***2011.***

[13] Verma, S, B., Stark, R. and Haidn, O., "**Reynolds Number Influence on Dual-Bell Transition Phenomena**", Journal of Propulsion and Power, Vol. 29, No. 3, DOI: 10.2514/1.B34734, ***May–June 2013***.

[14] Davis, K. and all, "**Experimental and Computational Investigation of a Dual-Bell Nozzle**", 53rd AIAA Aerospace Sciences Meeting, ***2014***.

[15] Schneider, D., Génin, C., Stark, R. and Fromm,C, M., "**Ariane 5 Performance Optimization Using Dual Bell Nozzle Extension**", Fourth Space Propulsion Conference, 3AF,. ***May 2014.***

[16] Schneider, D. and Génin, C., "**Numerical Investigation of Flow Transition Behavior in Cold Flow Dual-Bell Rocket Nozzles**", Journal of Propulsion and Power, DOI: 10.2514/1.B36010. ***May 2016.***

[17] Hamitouche, T. and all, "**Développement d'une méthode de conception de profils de tuyères doubles galbes (dual bell-nozzles)**", *2nd International*

Conference on Aeronautics Sciences. ICAS-02. ***November 2015***, Oran, Alegria.

[18] Kbab, H. and all, "**Design and performance evaluation of a dual bell nozzle**", Acta Astronautica 130 (2017) 52–59, http://dx.doi.org/10.1016/j.actaastro.2016.10.015, ***2017***.

[19] Hamitouche, T. and all, "**Design and Performances of the Dual-Bell Nozzle**", DOI:10.1109/AERO.2016.7500518, 2016 IEEE Aerospace Conference, ***05 - 12 March 2016***, Big Sky, MT, USA.

[20] ZMIJANOVIC, V., "**Secondary injection fluidic thrust vectoring of an axisymmetric supersonic nozzle**", PhD thesis, Université d'Orléans, France, ***2013***.

[21] Delery, J., "**Aérodynamique interne: tuyères et arrières corps**", ENSAE, Toulouse, 3rd éd. Revue et corrigée, ***1996***.

[22] Sauer, A., "**General Characteristics of the Flow through Nozzles at Near Critical Speeds**", NACA TM-1147, ***1947***.

[23] Zukrow, M, J. and Hofman, J, D. "**Gas Dynamics**", John Wiley & Sons, New York, ***1976***.